

Final report for Project **1200**

Project title: **Neogene Paleoelevation and Paleoclimate of the Central Alps**

Principal investigator: **Todd Ehlers**

Report period: **Jan. 1, 2021 - Dec. 31, 2021**

The project aims to integrate stable isotope altimetry records ( $\delta^{18}\text{O}/\delta\text{D}$ ) of the Central Alps with a high-resolution, global, isotope-enabled paleoclimate model. We use a high-resolution isotope-enabled general circulation model ECHAM5-wiso with Middle Miocene boundary conditions to investigate temperature, precipitation, and precipitation  $\delta^{18}\text{O}$  ( $\delta^{18}\text{O}_p$ ) changes. Experiments were designed with varied Alps elevations and  $\text{CO}_2$  levels to examine the influence of Alps surface uplift and global climate forcing effects on regional climate patterns and  $\delta^{18}\text{O}_p$ .

### **Experiments performed in 2021**

During this project we performed nine new ECHAM5-wiso experiments with Middle Miocene boundary conditions. The summary of the experiments is shown in Table 1.

First, we conducted two experiments with Middle Miocene boundary conditions reflecting two  $p\text{CO}_2$  settings (278 ppm and 450 ppm; Mio\_278 and Mio\_450 experiments) within current estimates of the Middle Miocene  $p\text{CO}_2$  [Foster and Rohling, 2013; Steinhorsdottir et al., 2021]. These two  $p\text{CO}_2$  settings approximately reflect MCO and MMCT climatic states, with Mio\_450 ppm representing the MCO and Mio\_278 representing MMCT. In addition to greenhouse gas concentrations ( $p\text{CO}_2$ ,  $p\text{CH}_4$ ,  $p\text{N}_2\text{O}$ ), the paleosimulations account for changing terrestrial ice sheets, vegetation cover, albedo, orbital variations, SSTs, and SICs (Table 1). We use the SSTs and SICs, generated by low-resolution fully coupled atmosphere-ocean COSMOS model experiments with Middle Miocene boundary conditions (Huang et al., [2017]; Starz et al., [2017]; their Mio\_278 and Mio\_450 experiments). Physical soil properties, such as soil albedo and maximum water holding field capacity are derived by adapting vegetation-related parameters computed by a dynamic vegetation module [Brovkin et al., 2009] of the global land surface and carbon cycle model JSBACH [Raddatz et al., 2007] as part the fully coupled atmosphere-ocean model COSMOS. Orography-related variables were derived from the paleogeographic reconstruction of Herold et al., [2008]. Although geography of the Middle Miocene and present are remarkably similar, the Middle Miocene reconstruction has several notable modifications, including rotation of continents, altered ocean gateways, and height of major orogens (Fig. 1).

Second, for both Middle Miocene  $p\text{CO}_2$  settings, we conduct three sensitivity experiments to investigate the effects of the Alpine topography and marine transgression/regression in Europe (Table 1, Fig. 1). We study the effects of uplift of the Alps by increasing and decreasing their elevation, similar to the pre-industrial sensitivity experiments. We reduce the elevation in the area covering the Alps and the Alpine forelands to 250 m elevation (Mio\_278\_noAlps, Mio\_450\_noAlps; Fig. S1 D) and increase the elevation to twice the reconstructed height (Mio\_278\_plusAlps, Mio\_450\_plusAlps; Fig. S1 E) compared to the original paleogeographic reconstruction of Herold et al., [2011], which reflects recent hypotheses of very high Alpine elevations in the Middle Miocene [Krsnik et al., 2021]. We also tested the influence of a marine transgression and regression within Europe on regional climate and stable water isotopes. For this purpose, we performed two additional experiments (Mio\_278\_SeaLand and Mio\_450\_SeaLand) with modified land-sea distributions over Europe (Fig. 1 F), corresponding to the mid-Middle Miocene reconstruction (14 Ma) from the Paleogeographic Atlas of the Paratethys region [Popov et al., 2004].

All experiments were performed at high resolution (T159 L31, corresponding to a grid spacing of  $\sim 0.75^\circ$ , or  $\sim 80$  km in latitude and longitude at the equator, with 31 vertical levels up to 10 hPa). The experiments reached a quasi-equilibrium state in the first three model years. We analyzed computed climatological values and inter-annual variations of the last 10 model years for each experiment.

**Table 1.** ECHAM5-wise experiments summary performed in 2021 under project 1200.

Experiment name	Greenhouse gases concentration	Orbital parameters	Surface conditions	Alps elevation
Mio_278	CO <sub>2</sub> 278 ppmv, CH <sub>4</sub> 650 ppbv, N <sub>2</sub> O 270 ppbv	eccentricity = 0.016724, obliquity = 23.4468, longitude of perihelion = 272.157	Sea surface temperature, sea ice and vegetation from Middle Miocene COSMOS (278 ppm) simulations [Stärz et al., 2017]. Paleogeography from Middle Miocene reconstruction (Herold et al 2011a). The height of the Antarctic ice-sheet is reduced compared to present-day (Herold et al., 2008), the Greenland ice-sheet is absent. We derived physical soil characteristics, such as soil albedo and maximum water holding field capacity by adapting vegetation related parameters based on (Stärz et al., 2017).	100% of present
Mio_278_noAlps	Same as Mio_278	Same as Mio_278	Same as Mio_278	reduced to 250 m
Mio_278_plusAlps	Same as Mio_278	Same as Mio_278	Same as Mio_278	increased by 100 %
Mio_278_LandSea	Same as Mio_278	Same as Mio_278	Same as Mio_278, except for the Paratethys Sea area which extends in accordance to Popov et al., (2012).	100% of present
Mio_450	CO <sub>2</sub> 450 ppmv, CH <sub>4</sub> 650 ppbv, N <sub>2</sub> O 270 ppbv	eccentricity = 0.016724, obliquity = 23.4468, longitude of perihelion = 272.157	Sea surface temperature, sea ice and vegetation from Middle Miocene COSMOS (450 ppm) simulations (Stärz et al., 2017). Paleogeography from Middle Miocene reconstruction (Herold et al 2011a). The height of the Antarctic ice-sheet is reduced compared to present-day (Herold et al., 2008), the Greenland ice-sheet is absent. We derived physical soil characteristics, such as soil albedo and maximum water holding field capacity by adapting vegetation related parameters based on (Stärz et al., 2017).	100% of present
Mio_450_noAlps	Same as Mio_450	Same as Mio_450	Same as Mio_450	reduced to 250 m
Mio_450_plusAlps	Same as Mio_450	Same as Mio_450	Same as Mio_450	increased by 100 %
Mio_450_LandSea	Same as Mio_450	Same as Mio_450	Same as Mio_450, except for the Paratethys Sea area which extends in accordance to Popov et al., (2012).	100% of present

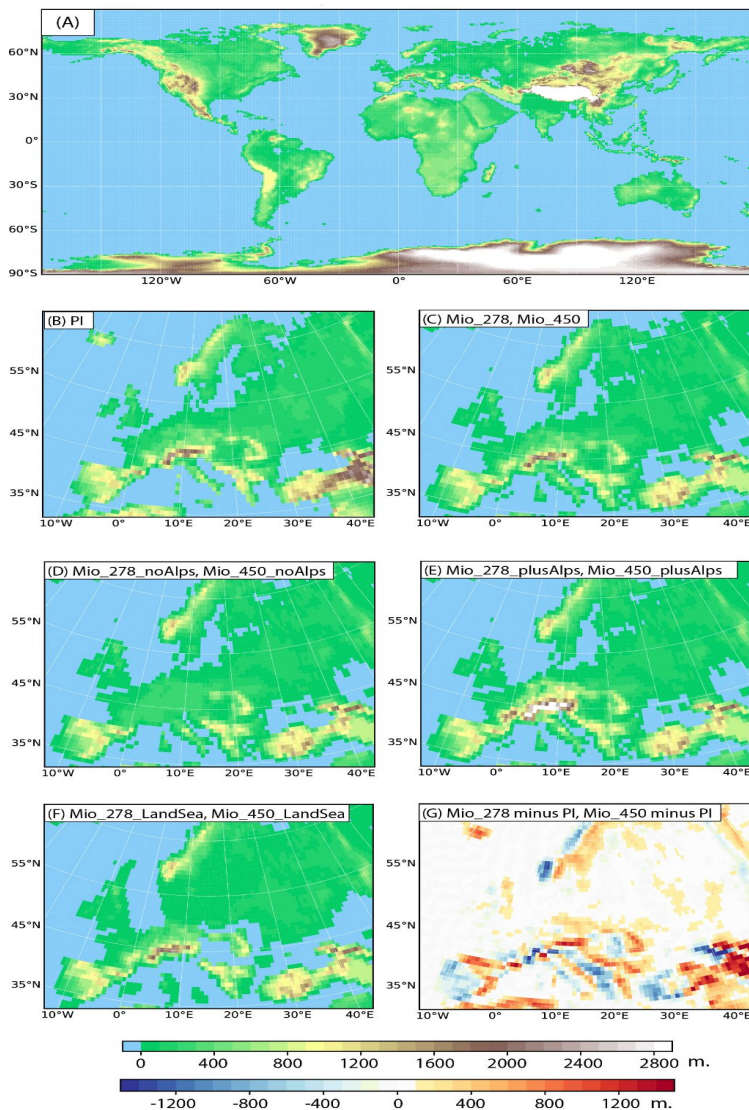


**Figure S1.** Global (A) middle Miocene paleogeography of Herold et al. (2008) at T159 model resolution, used in Mio\_450 and Mio\_278 experiments; (B) Present-day topography for Europe at T159 model resolution, (C) same as subplot A but for the European region; (D) modified paleogeography of the Middle Miocene with Alpine elevation reduced to 250 m compared to the original reconstruction of Herold et al. (2008), applied in Mio\_450\_noAlps and Mio\_278\_noAlps experiments; (E) modified paleogeography of the middle Miocene with increased Alpine elevation by 100% compared to the original reconstruction of Herold et al. (2008), applied in the Mio\_450\_plusAlps and Mio\_278\_plusAlps experiments; (F) modified paleogeography of the Middle Miocene, with the land-sea distribution in the European region according to Popov et al., (2012), applied in Mio\_278\_LandSea and Mio\_450\_LandSea experiments; (G) topography difference between Mio\_278/Mio\_450 experiments and present-day in the European region.

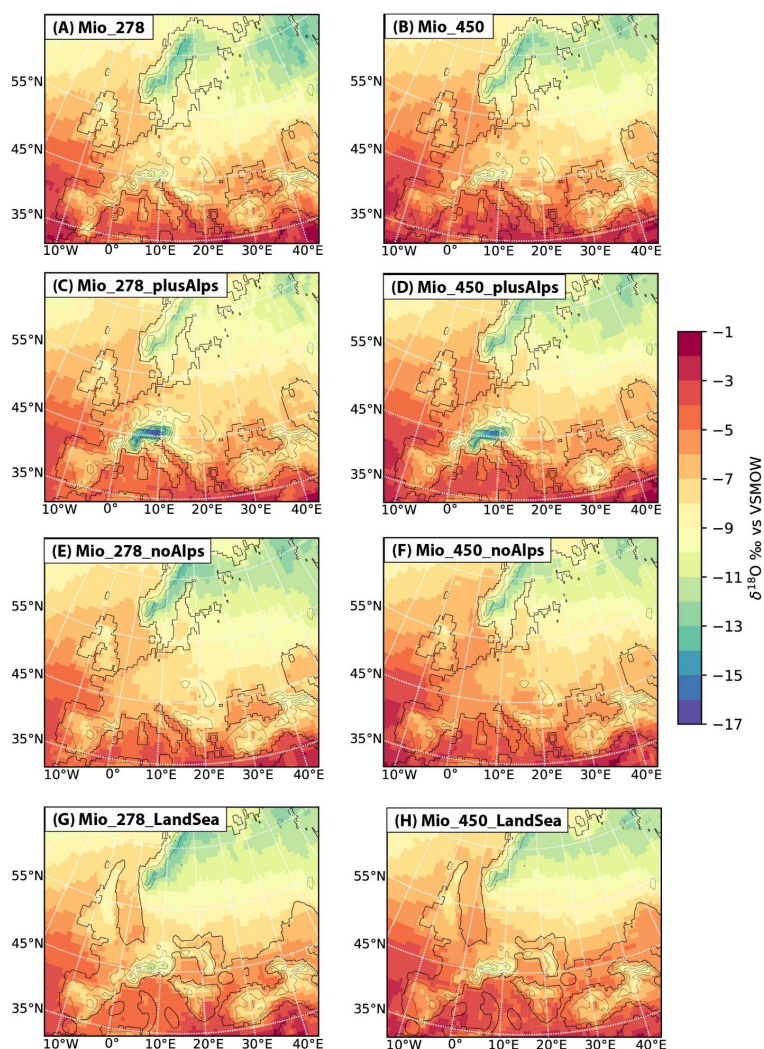
## Results

We presented high-resolution isotope-enabled ECHAM5-wiso experiments to study Middle Miocene climate and the related  $\delta^{18}\text{O}_p$  signals in Europe. Previous modelling efforts simulating Middle Miocene climate have been recently joined in MioMIP1 and summarized in *Burls et al.* [2021]. However, low resolution of MioMIP1 simulations (T31 or T42) do not provide a good representation of mountain topography in Europe, leading to: 1) an underestimation of surface temperature in mountain regions, and 2) an underestimation of precipitation. Moreover, it has been previously shown that the low resolutions (e.g., T31), typical of past global coupled paleoclimate simulations, are unlikely to properly capture humidity behavior [*Sherwood et al.*, 2010].

We have tackled this problem in generating much higher resolution simulations with ECHAM5-wiso atmosphere general circulations model. Our new Middle Miocene simulations show 3.4 - 6.2 °C higher temperature in central Europe than for the pre-industrial, depending on the CO<sub>2</sub> setup. This result is in good agreement with temperatures derived using the coexistence approach proxy data, however, have warm bias for low-elevation areas when comparing to the Middle Miocene experiments participating in the MioMIP1 project. The simulated Middle Miocene precipitation is 300 - 500 mm/year lower over the central Europe than pre-industrial and is consistent with estimates from heterafaunal fossil proxy data. However, it is lower than predicted by the coexistence approach proxy data. We attribute this precipitation change in Europe to shifts in large-scale pressure patterns in the North Atlantic and over Europe, namely anticyclonic circulation centered over the Mediterranean and Southern Europe in winter, in

addition to a deepened Icelandic Low in the summer. These ultimately result in a northward shift of the Atlantic storm track with a deflection of storms north of the Mediterranean into higher latitudes.

The simulated annual mean  $\delta^{18}\text{O}_p$  pattern for the Middle Miocene is consistent with pre-industrial  $\delta^{18}\text{O}_p$  across Europe in both its pattern and magnitude (Fig. 2). The Middle Miocene global climate forcing has contributed to a maximum  $\delta^{18}\text{O}_p$  increase of  $\sim 2\text{‰}$  over the high Alpine elevation and to  $\sim 1\text{‰}$  over low elevation. However, differences between PI and Middle Miocene



simulations at seasonal scale are stronger ( $\sim 3\text{‰}$ ), especially when higher  $p\text{CO}_2$  concentration is considered. The most striking is the  $\delta^{18}\text{O}_p$  decrease in late summer, driven by a drop of relative humidity, which coincides with enhanced atmospheric subsidence. Experiments with varied elevations of the Alps show that an increase by 100 % of Alps elevation causes a maximum  $\delta^{18}\text{O}_p$  decrease, up to 8 ‰ when compared to the experiment with non-changed topography. However, the isotope lapse rate in the Central Alps of  $0.03 \text{‰}/100 \text{ m}$  shallows for a high  $p\text{CO}_2$  Middle Miocene setting.

**Figure 2.** Annual averaged  $\delta^{18}\text{O}_p$  for (A) Mio\_278, (B) Mio\_450, (C) Mio\_278\_plusAlps, (D) Mio\_278\_plusAlps, (E) Mio\_278\_noAlps, (F) Mio\_450\_noAlps, (G) Mio\_278\_LandSea, (H) Mio\_450\_LandSea.

### Publication (in revision with co-authors):

Botsyun S., Ehlers T. A., Koptev A., Böhme M., Methner K., Risi C., Stepanek C., Werner M., Mutz S. G., Boateng D., Mulch A. Middle Miocene climate and stable oxygen isotopes in Europe based on numerical modeling. In preparation for *Paleoceanography and Paleoclimatology*.

### References

- Brovkin, V., T. Raddatz, C. H. Reick, M. Claussen, and V. Gayler (2009), Global biogeophysical interactions between forest and climate, *Geophys. Res. Lett.*, 36(7).
- Burls, N. J., C. D. Bradshaw, A. M. De Boer, N. Herold, M. Huber, M. Pound, Y. Donnadieu, A. Farnsworth, A. Frigola, and E. Gasson (2021), Simulating Miocene warmth: insights from an opportunistic Multi-Model ensemble (MioMIP1), *Paleoceanogr. Paleoclimatology*, e2020PA004054.
- Foster, G. L., and E. J. Rohling (2013), Relationship between sea level and climate forcing by  $\text{CO}_2$  on geological timescales, *Proc. Natl. Acad. Sci.*, 110(4), 1209–1214.

- Herold, N., M. Seton, R. D. Müller, Y. You, and M. Huber (2008), Middle Miocene tectonic boundary conditions for use in climate models, *Geochemistry, Geophys. Geosystems*, 9(10), doi:10.1029/2008GC002046.
- Herold, N., M. Huber, and R. D. Müller (2011), Modeling the Miocene climatic optimum. Part I: Land and atmosphere, *J. Clim.*, 24(24), 6353–6372.
- Huang, X., M. Stärz, K. Gohl, G. Knorr, and G. Lohmann (2017), Impact of Weddell Sea shelf progradation on Antarctic bottom water formation during the Miocene, *Paleoceanography*, 32(3), 304–317, doi:10.1002/2016PA002987.
- Krsnik, E., K. Methner, M. Campani, S. Botsyun, S. G. Mutz, T. A. Ehlers, O. Kempf, J. Fiebig, F. Schlunegger, and A. Mulch (2021), Miocene high elevation and high relief in the Central Alps, *Solid Earth Discuss.*, 1–28.
- Popov, S. V., F. Rögl, A. Y. Rozanov, F. F. Steininger, I. G. Shcherba, and M. Kovac (2004), Lithological-paleogeographic maps of Paratethys-10 maps late Eocene to pliocene,
- Raddatz, T. J., C. H. Reick, W. Knorr, J. Kattge, E. Roeckner, R. Schnur, K.-G. Schnitzler, P. Wetzell, and J. Jungclaus (2007), Will the tropical land biosphere dominate the climate–carbon cycle feedback during the twenty-first century?, *Clim. Dyn.*, 29(6), 565–574.
- Sherwood, S. C., W. Ingram, Y. Tsushima, M. Satoh, M. Roberts, P. L. Vidale, and P. A. O’Gorman (2010), Relative humidity changes in a warmer climate, *J. Geophys. Res. Atmos.*, 115(D9).
- Stärz, M., W. Jokat, G. Knorr, and G. Lohmann (2017), Threshold in North Atlantic-Arctic Ocean circulation controlled by the subsidence of the Greenland-Scotland Ridge, *Nat. Commun.*, 8, 15681.
- Steinhorsdottir, M., H. K. Coxall, A. M. De Boer, M. Huber, N. Barbolini, C. D. Bradshaw, N. J. Burls, S. J. Feakins, E. Gasson, and J. Henderiks (2021), The Miocene: The future of the past, *Paleoceanogr. Paleoclimatology*, 36(4), e2020PA004037.